Proceedings of the ASME 2019
International Design Engineering Technical Conferences
and Computers and Information in Engineering Conference
IDETC/CIE2019
August 18-21, 2019, Anaheim, CA, USA

DETC2019-97435

DYNAMIC TRANSFORMATION OF AN ORIGAMI STRING USING A STACKED-MIURA CELL

Chang Liu
Mechanical & Industrial Engineering
Northeastern University
Boston, Massachusetts 02115
Email: liu.chang7@husky.neu.edu

Zwe Min Htet Aung
Mechanical & Industrial Engineering
Northeastern University
Boston, Massachusetts 02115
Email: aung.z@husky.neu.edu

Samuel M. Felton[*]
Mechanical & Industrial Engineering
Northeastern University
Boston, Massachusetts 02115
Email: s.felton@northeastern.edu

ABSTRACT

Origami engineering is a promising approach to transforming structures and machines due to its potential for geometric, kinematic, and mechanical complexity. However, actuating this transformation can be expensive, slow, and unreliable. In this paper, we demonstrate repeatable and reversible transformation of a two-vertex origami string between different configurations using a stacked-Miura cell as an actuation system. We characterize the snap-through behavior of the cell and show how the cell can be coupled to the string to generate drive repeatable transformations between different configurations. We then show how gravity can affect this process. The results indicate that bistable origami cells are a promising method for lightweight, repeatable transformation.

NOMENCLATURE
P   Parallel configuration
AP   Antiparallel configuration

INTRODUCTION

Origami folds are capable of creating complex three-dimensional structures from sheet materials. This technique has been used to build origami-inspired machines with capabilities including transformable geometries [1, 2], programmable mechanical properties [3,4], and facile manufacturing [5–7]. Particularly relevant to this paper, origami engineering has been proposed as a functional approach to transformation. This concept has been applied to structures and machines, with applications including robotics [8–10], space exploration [11, 12], and wireless communication [13, 14].

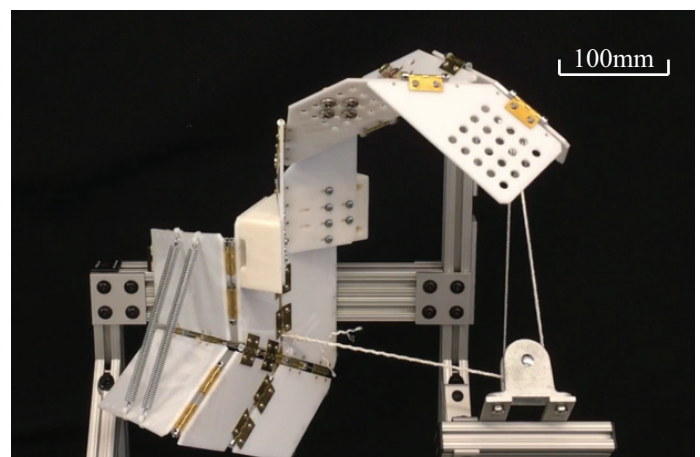However, we currently lack a method for actuating trans-

FIGURE 1: A TWO-VERTEX ORIGAMI STRING DRIVEN BY A STACKED-MIURA CELL.

---

[*]Address all correspondence to this author.

formation that is efficient, cost effective, and reliable. Previous efforts have focused on self-folding, in which low-profile functional materials are embedded within the structure. Examples of these materials include shape memory polymers [15, 16], shape memory alloys [1, 17], and swelling hydrogels [18–21]. These increase complexity and cost of the structure and are often difficult to control. Moreover, self-folding at a large (centimeter to meter) scale [8, 22] happens at a slower pace, lasting from minutes to hours. Other techniques such as the use of pneumatic pouch motors [10, 22, 23] lack folding accuracy, and using DC motors [24, 25] to power them requires bulky mechanisms and an external power supply.

These challenges are particularly relevant when the transformation occurs near the flat-unfolded state. In this state, an origami pattern is in a kinematic singularity, and can often fold into multiple configurations, each with their own kinematic behavior and mechanical behavior [26, 27]. If a self-folding structure enters the wrong configuration, it can become locked in an ineffective state [28].

An alternative method for transforming origami structures is to take advantage of the origami string's dynamic behavior. Zuliani *et al.* [24] showed that an origami structure would transform between multiple configurations when actuated at different frequencies, and Liu *et al.* [25] devised a model to predict these transformations in response to a step input. In summary, an origami structure with a single kinematic degree of freedom but multiple configurations could reliably transform using only a single actuator. However, due to the dynamic nature of the transformation, this required a relatively high-power input driven by an electric motor that was substantially heavier than the origami structure.

To replace the electric motor with a lightweight mechanism that can still deliver a large impulse to the origami structure, we looked to bistable mechanisms to provide this dynamic excitation and drive transformation. One promising origami-inspired design is the The stacked-Miura cell, which was studied to mimic the behavior of plants that move without muscles [29–31]. It is made up of two connected Miura folds that exhibit bi-stable behavior when designed with the required constraints [29, 32]. The system is designed to store elastic potential energy at the unstable point where the cell can "snap" into either configuration with a fixed speed without the need for separate actuation mechanisms [29]. There are simpler bistable mechanisms, Existing including buckled beams [33], but stacked-Miura cells have the following advantages to our application: (1) They are also origami-based, making their design and fabrication inherently compatible with origami transformation; (2) They have multiple angles which can act as different 'outputs' for different components; and (3) They can be connected into arrays of coupled units, allowing for distributed actuation of larger systems.

In this paper, we present the design and characterization of an origami string with transformation driven by an integrated stacked-Miura cell to generate dynamic excitations to transform an origami string. The cell's bistable behavior results in a repeatable dynamic input to the base of the origami string. We show that the resulting transformation is reliable, reversible, and can be modified by changing the stiffness of the cell or orientation of the string (and gravity's effect on its dynamics). With this capability we can create origami systems that can rapidly transform into specific configurations without power-intensive actuation (Fig. 1).

DESIGN AND MODELING

Our system consists of two components: an origami string that can transform into distinct configurations, and a stacked-Miura cell that can provide specific dynamic excitations to the origami string. The origami string can transform among configurations when the base input passes through the flat state and the stacked-Miura cell provides an angular displacement as input. In order to couple the origami string and the stacked-Miura cell, an angle offset is introduced.

Origami String

Design Previous studies have defined the Miura vertex as an origami pattern made out of four plates and connected with four creases. [11]. Among the four creases, the two spinal creases (in red) are collinear when flat and the two peripheral creases (in blue) are symmetric across the spine with an angle α between the spinal and peripheral creases as shown in Fig. 2(A). When this Miura vertex folds, we define the lower spinal angle as θ_1, upper
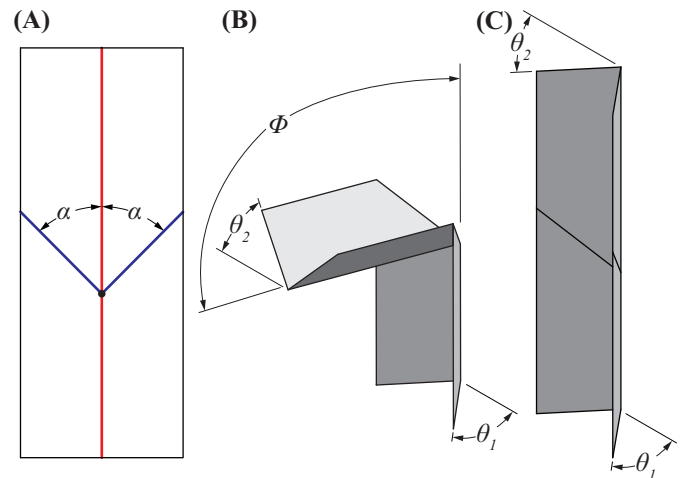

FIGURE 2: MIURA VERTEX DESIGN. (A) MIURA CREASE PATTERN, RED: SPINAL CREASES, BLUE: PERIPHERAL CREASES. (B) ANTIPARALLEL (AP) CONFIGURATION. (C) PARALLEL (P) CONFIGURATION.
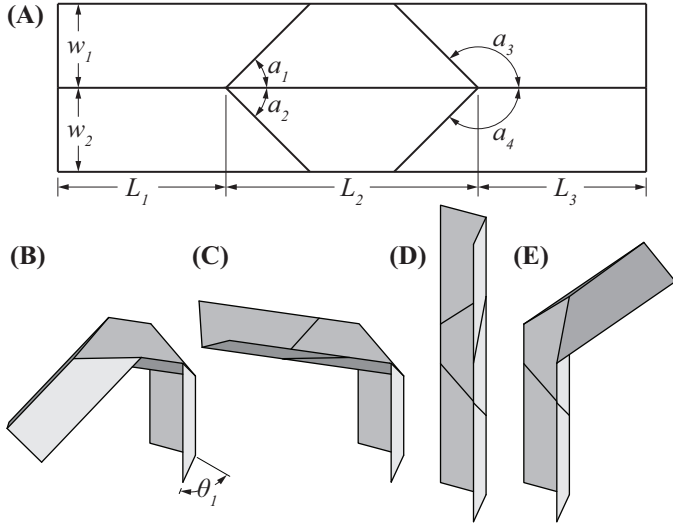
FIGURE 3: ORIGAMI STRING DESIGN. (A) A TWO VERTICES MIURA-ORIGAMI PATTERN. (B-E) FOUR DISTINCT CONFIGURATIONS THE ORIGAMI STRING CAN ACHIEVE. (B) ANTIPARALLEL-ANTIPARALLEL CONFIGURATION. (C) ANTIPARALLEL-PARALLEL CONFIGURATION, (D) PARALLEL-PARALLEL CONFIGURATION. (E) PARALLEL-ANTIPARALLEL CONFIGURATION.

spinal angle as θ_2 and segment angle as ϕ. Based on the relation between θ_1 and θ_2, we define two configurations, antiparallel (AP) configuration when $\theta_1 = -\theta_2$ with $\phi > 0$ (Fig. 2(B)), and parallel (P) configuration when $\theta_1 = \theta_2$ with $\phi = 0$ (Fig. 2(C)).

One class of origami structures that use the Miura vertex pattern is the origami string [34]. The string consists of multiple Miura vertices connected in series, all sharing a single degree of freedom. The trajectory of the string can be programmed by changing its fold angle or the angles between the hinges at each vertex, and can approximate any path in 3D space. In this paper we use a two-vertex string (Fig. 3(A)). This string can fold into four distinct configurations with different mount-valley assignments to its hinges (eight, if considering their symmetric configurations), as shown in Fig. 3(C-D). Using a naming convention in which the lower vertex configuration is followed by the upper vertex configuration, we name the four configurations as 'antiparallel-antiparallel' (AP-AP) (Fig. 3(B)), 'antiparallel-parallel' (AP-P) (Fig. 3(C)), 'parallel-parallel' (P-P) (Fig. 3(D)) and 'parallel-antiparallel' (P-AP) (Fig. 3(E)) respectively. In our physical system, we use $L_1 = L_3 = 75\,$mm, $L_2 = 225\,$mm, $w_1 = w_2 = 75\,$mm, $\alpha_1 = \alpha_2 = 45°$, and $\alpha_3 = \alpha_4 = 135°$.

Concept of Dynamic Transformation During transformation of an origami string, the final configuration depends

on its initial configuration, angular input signal (velocity and displacement), body forces (e.g. gravity) and the inertia and stiffness of its components. Previous studies have validated a physics-based model that lumps several dynamic parameters into a set of inertia and stiffness values for each vertex [25]. The general concept of this model is that the origami string is not kinematically constrained, but instead can be considered a series of state variables (angles) with inertia and connected by springs. Due to the backlash in the system, there is a phase lag between output angle θ_2 and input angle θ_1 of each vertex (referring to Fig. 2). When the vertex passes through the flat state and θ_1 changes sign, this phase lag creates a 'window' in which when θ_2 hasn't yet changed sign and transformation could occur. In order for the mechanism to stay in the same configuration, θ_2 must also cross the flat state and change sign to match θ_1. In order for θ_2 to pass through flat state, The kinetic energy of the vertex, determined from its inertia and speed, must be greater than its potential energy defined by its stiffness and starting position.

Stacked-Miura Cell

The fundamental components of the stacked-Miura cell are two Miura vertices (Fig. 4(A)). There are some constraints, $b_1 = b_2$ and $\frac{\cos\beta_1}{\cos\beta_2} = \frac{a_2}{a_1}$, that must be satisfied in order to make the two folds kinematically compatible (as in Fig. 4(B)) as shown in Li *et al.* [29].

Here we define the fold direction as 'out' when the inner volume increases (transform from Fig. 4(D) to Fig. 4(C)), and 'in' when the inner volume decreases (transform from Fig. 4(D) to Fig. 4(E)). We define the folding angle of the peripheral crease of the upper Miura vertex as η (Fig. 4(C-E)). When stacked-Miura cell folds out, η changes from an obtuse angle to a acute angle. In our physical system, we use $a_1 = 100\,$mm, $a_2 = 175\,$mm, $b_1 = b_2 = 100\,$mm, $\beta_1 = 60°$ and $\beta_2 = 73.4°$.

Previous studies have provided us the kinematic relationship of the angles in the stacked-Miura cell [29] that enable snap-through behavior and bi-stability. Here we use angle η (Fig. 4) as the dynamic input for origami string since it passes through flat state ($\eta = 180°$) and settles down in one of the stable states due to the potential energy stored in the stacked-Miura cell mechanism.

Coupling Origami String to Stacked-Miura Cell

To make the dynamic behavior as repeatable as possible, the cell is driven at a negligible velocity up to the snap-through point $\eta = 180°$ (Fig. 5(B)) and allowed to snap freely through based on its inherent stiffness and inertia. Because of this, we assume that the velocity of angle η is zero ($\dot{\eta}_{(\eta=180°)} \approx 0$) when the cell reaches the snap-through point. If we mount the origami string directly to the stacked-Miura cell at angle η, the origami string won't obtain a velocity when the input passes through flat state. To solve this problem, we manually added an angle offset ε to
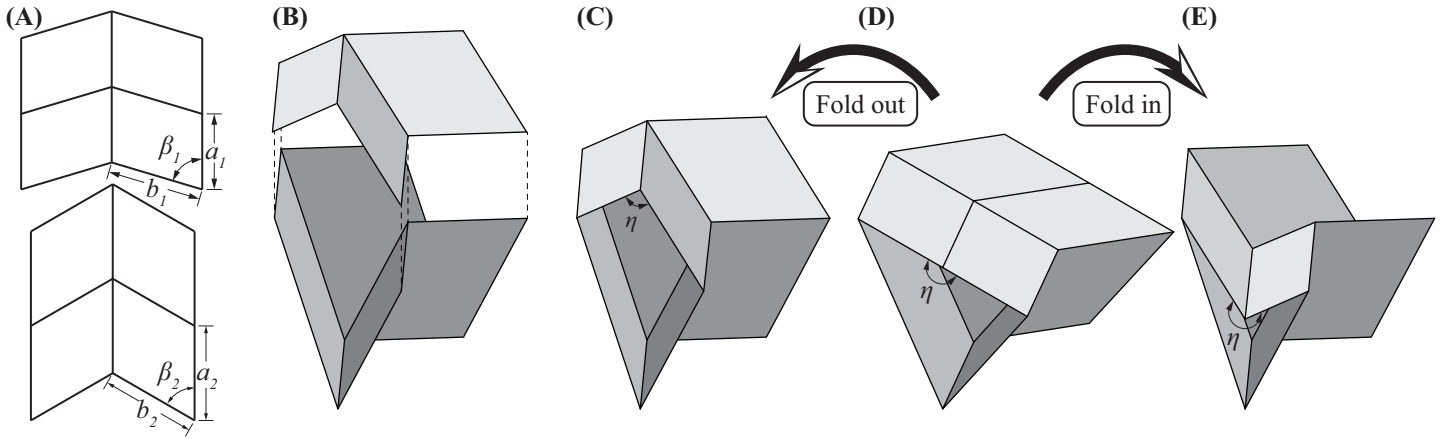
FIGURE 4: STACKED-MIURA CELL DESIGN. (A) MIURA-ORIGAMI PATTERNS OF THE TWO PLATES. (B) THE TWO PLATES ARE STACKED TOGETHER. (C-E) STACKED-MIURA CELL FOLDS 'OUT' WHEN INNER VOLUME INCREASES AND FOLDS 'IN' WHEN INNER VOLUME DECREASES.

input angle θ_1, where $2\varepsilon + \eta - 180 = 2\theta_1$ (Fig. 5(A)). We 3D printed the blocks (using Form 2, Formlabs, White Resin 1L, RS-F2-GPWH-04) and mounted it onto the stacked-Miura cell (Fig. 5(D)). This design feature puts the origami string at a position such that it passes through the flat state (Fig. 5(C)) when the stacked-Miura cell achieves maximum angular velocity.

FABRICATION

To fabricate the origami string and stacked-Miura cell, we used 3 mm-thick acrylic sheets as the structural plate material and barrel hinges between adjacent plates. Individual plates were cut using a CO_2 laser cutter (Universal Laser Systems, PLS6M2). Surface-mount barrel hinges (McMaster-Carr #1603A23) with
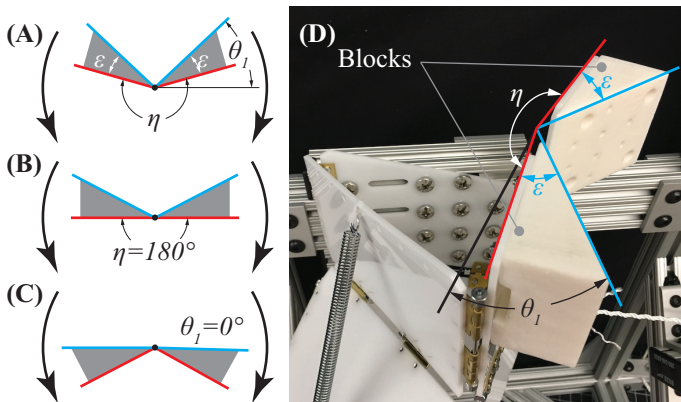

FIGURE 5: WORKING PRINCIPLE OF THE PHASE LAG. (A) INITIAL STATUS, WHERE ANGLE η HAS NOT PAST THROUGH FLAT UNFOLD STATE. (B) WHEN η PASSES THROUGH FLAT UNFOLD STATE, ORIGAMI STRING IS STILL IN ITS INITIAL CONFIGURATION WITH INPUT ANGLE θ_1. (C) THE BASE OF ORIGAMI STRING PASSES THE FLAT UNFOLD STATE WHEN η HAS REACHED FULL SPEED. (D) A PHOTO OF THE TEST SET-UP, WITH TWO BLOCKS MOUNTED ON THE STACKED-MIURA CELL TO PROVIDE THE ANGLE OFFSET ε, WHERE $2\varepsilon + \eta - 180 = 2\theta_1$.
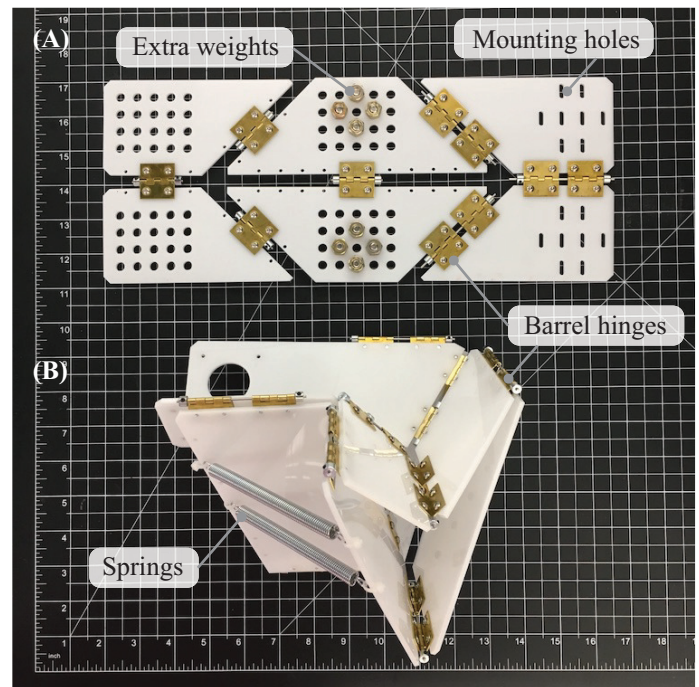

FIGURE 6: (A) ORIGAMI STRING. (B) STACKED-MIURA CELL. THE WIDTH OF THE SQUARE GRID IS 12.7 MM.

4

5/64" diameter pins were first dissembled by knocking the pins out. The pairs of separated leaves were then screwed to the adjacent plates, reconnected by using 1/16" diameter rotary shaft and locked using set-screw shaft collars (McMaster-Carr #6432K71). We used shafts with a slightly smaller diameter in order to increase flexibility of the original surface-mount barrel hinges, reduce friction and provide the backlash necessary for Miura vertex transformation.

For the origami string component (Fig. 6(A)), holes were cut on the facets. Holes on the two plates on the right were used to mount the origami string to the stacked-Miura cell, while holes on the four facets on the left were used to mount weights (1/4"-20 screws and nuts) that increase inertia of the origami string. The number of barrel hinges on each crease was varied to adjust stiffness. For the stacked-Miura cell component (Fig. 6(B)), an elastic element was mounted to the stacked-Miura cell using cable ties (McMaster-Carr #7130K53) in order to generate bistability.

EXPERIMENTS AND RESULTS

We first characterized the dynamic behavior of the origami cell when built with different inherent stiffnesses. We then mounted an origami string to the stacked-Miura cell, quasi-statically pushed the cell to the bistable point and allowed it to snap through freely while observing the resulting transformation.

Dynamic Behavior of Stacked-Miura Cell

Previous studies have shown that the stacked-Miura cell has a critical, unstable equilibrium configuration at $\eta = 180°$ [29]. This is the point at which the mechanism has a local maximum potential energy and will snap to one of the two configurations. Here we studied the dynamic behavior of the stacked-Miura cell by characterizing the angle η when the mechanism snaps through the unstable equilibrium configuration.

The stacked-Miura cell mechanism was mounted on a frame made with 80-20 and a high speed camera (SONY Cyber-shot RX100V, 960fps) was placed over the hinge corresponding to η. The mechanism was actuated using a tendon driven system as shown in Fig. 1. The tendon was pulled slowly so as not to affect the dynamic response. Angle η in each frame was tracked using a MATLAB program.

TABLE 1: FULL SPEED ANGLES AND ANGULAR SPEED.

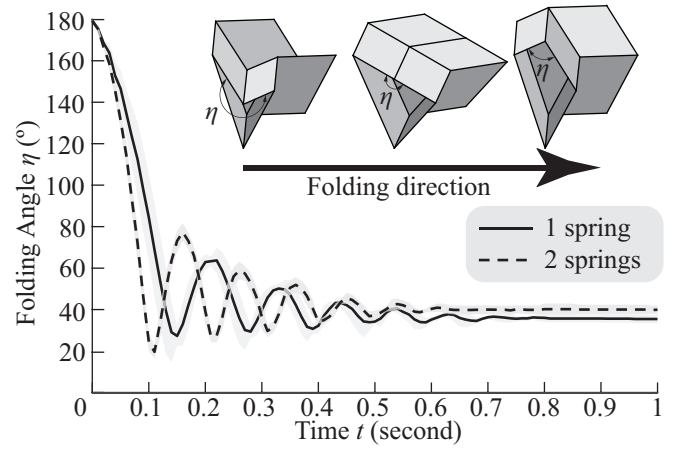| # of springs	Full speed angle η_{fs} (°)	Angular speed $\dot{\eta}$ (rad s^{-1})	Related plot
1	131.31±1.10	25.68±0.12	Fig. 7 Solid
2	135.77±1.79	38.97±0.16	Fig. 7 Dashed

FIGURE 7: STACKED-MIURA CELL OUTPUT ANGLE η AS A FUNCTION OF TIME WHEN VARYING THE NUMBER OF SPRINGS. SOLID LINE: ONE SPRING HOOKED ON THE STACKED-MIURA CELL. DASHED LINE: TWO SPRINGS HOOKED ON THE STACKED-MIURA CELL. SHADED AREAS INDICATE STANDARD DEVIATION. $N = 3$

We varied the number of elastic elements to create different dynamic responses, installing one or two springs across the cell. Results of tracked angle η are shown in Fig. 7. The left edge of the plot ($t = 0$ s) represents the snap-through point, where $\eta = 180°$. As shown in the results, with more elastic elements, the stacked-Miura cell accelerates faster and reaches a higher velocity due to higher potential energy stored in the system at the unstable equilibrium configuration (the snap-through point). For each response, an angle η_{fs} was identified as the point at which the angular velocity $\dot{\eta}$ became effectively constant. These values are summarized in Tab. 1.

In both cases, we observed that $\eta_{fs} \approx 130°$. Therefore, when attaching the origami string in future experiments we chose to use an angle offset of $\varepsilon = 27.5°$ so that the system would reach a constant velocity by the time the origami string reached the flat state.

Origami String Transformation

To demonstrate the transformation of a two-vertex origami string using the stacked-Miura cell, we mounted the string onto the cell (Fig. 8). The origami string was initially placed in AP-AP configuration, defined in Fig. 3. When actuating the stacked-Miura cell with the single spring, the string transformed from the AP-AP to the AP-P configuration (Fig. 8(A)). When the cell had two springs installed, the string transformed from AP-AP to P-P (Fig. 8(B)). Each of these experiments were run 10 times and the same transformation occurred in each case, indicating that the
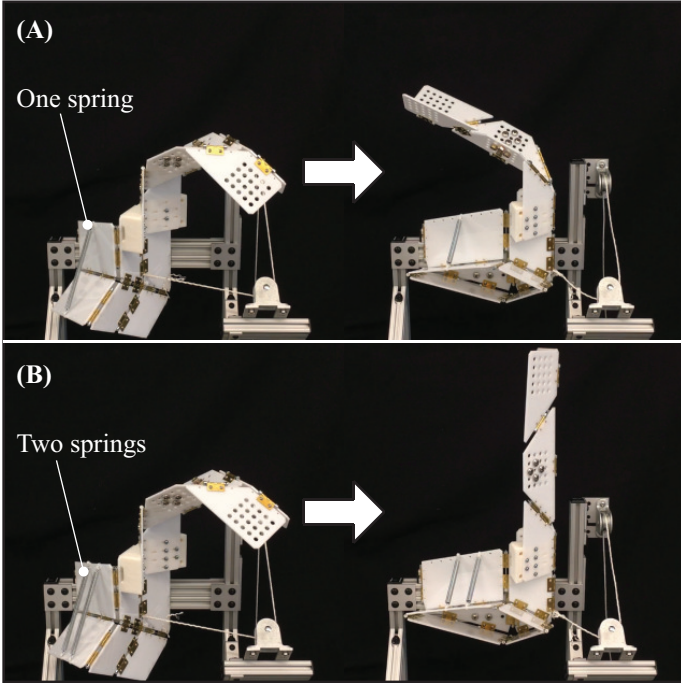
FIGURE 8: ORIGAMI STRING TRANSFORMATION. (A) TRANSFORMATION DRIVEN BY THE STACKED-MIURA CELL WITH ONE SPRING. (B) TRANSFORMATION DRIVEN BY THE STACKED-MIURA CELL WITH TWO SPRINGS. $N = 10$.

FIGURE 9: PHASE LAG OF THE LOWER VERTEX. DASHED LINE INDICATES CRITICAL PHASE LAG ANGLE θ_B. ERROR BARS INDICATE STANDARD DEVIATION. $N = 10$.

transformation is repeatable.

To better understand this transformation, we placed a high speed camera (SONY Cyber-shot RX100V, 960fps) in front of the structure to capture the angular displacement of the hinges over time. The phase lag $(\theta_2 - \theta_1)_{\theta_1 = 0°}$ of the lower vertex was measured and results are shown in Fig. 9. We can see that phase lag is greater when actuated with two springs than with one spring. In addition, we calculated the zero-torque displacement (backlash) θ_b of the string by holding the lower plates flat and vertical, and observed that that θ_2 settled down at $\theta_b = 5.25°$. This angle is marked in in Fig. 9 as a dashed line. Because θ_2 can move freely within the backlash range $\theta_1 \pm \theta_b$, we expect that as long as the phase lag is less than θ_b transformation will not occur during pass-through, such as in the lower vertex in Fig. 8(A). However, if the phase lag is greater than θ_b, then θ_2 gets 'locked' before it can pass through the flat state and the vertex transforms, such as the lower vertex in Fig. 8(B). Note that this behavior occurs in each vertex, so separate measurements would need to be collected on the upper vertices to further validate the model.
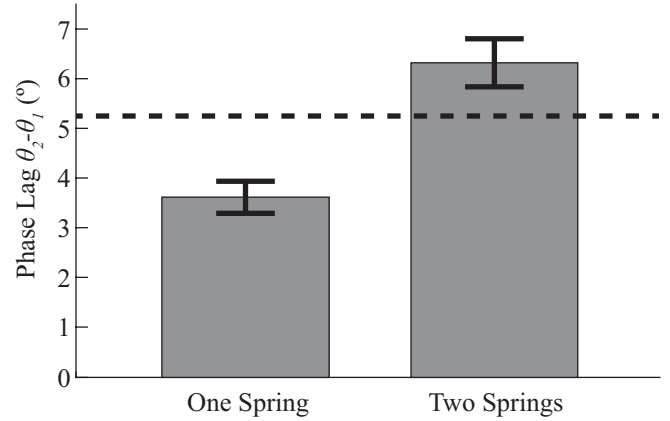
Reversibility Implementation

Due to the angle offset between the origami string base and the stacked-Miura cell, the snap-through only excites the origami string when the stacked-Miura cell folds out. In the opposite direction, the slow actuation means that the dynamics are negligible, and in the absence of body forces transformation would be unpredictable. However, due to the weight of the origami string, gravity plays an important role in transformation especially during this quasi-static motion. To demonstrate gravity's effect on transformation, we tilted the mechanism by $-4.4°$ (Fig. 10(A)) and $4.4°$ (Fig. 10(B)) and applied the same tendon-driven actuation, but repeated it in both directions for several cycles. We found out that when we tilted the mechanism by $-4.4°$, as shown in Fig. 10(A), the origami string transformed from AP-AP configuration to AP-P configuration when fast dynamic excitation was applied, and reversed when slow dynamic excitation was applied. Moreover, when we tilted the mechanism by $4.4°$ and provided sequential dynamic excitations to the origami string, it transformed through four different configurations and back to its initial configuration (Fig. 10(B)). In both cases, each cycle was performed 10 times with identical transformations, indicating the repeatability of the process.

CONCLUSION AND DISCUSSION

In this paper, we demonstrated the use of an origami structure as an actuator capable of generating rapid angular excitation. By changing the number of elastic elements installed in the stacked-Miura cell, we can control energy storage that changes dynamic behavior in the stacked-Miura cell mechanism when it snaps through the unstable equilibrium state. By utilizing the stacked-Miura cell mechanism, we achieved repeatable
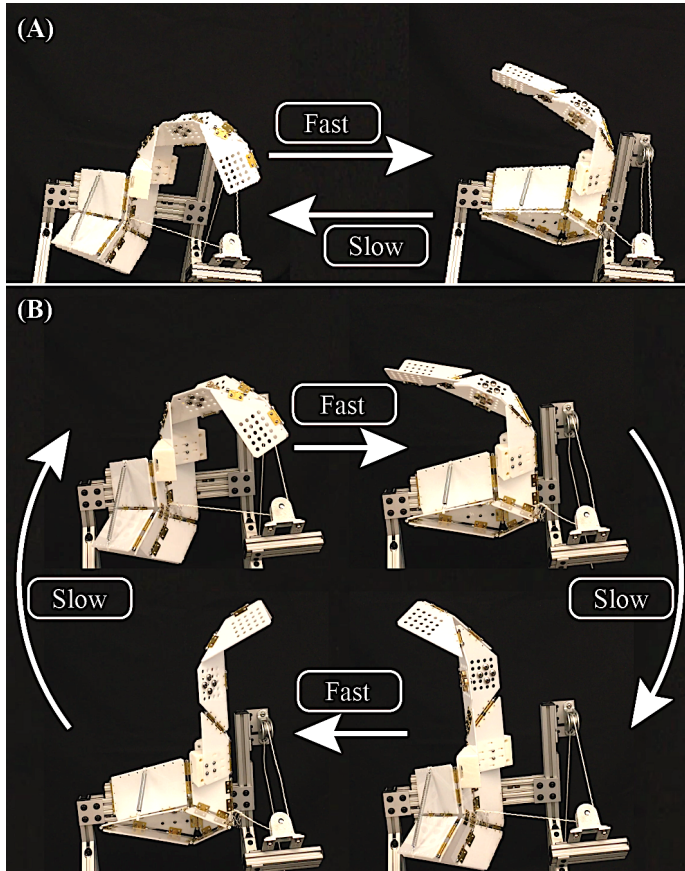
6

FIGURE 10: REVERSIBLE TRANSFORMATION WHEN THE ORIGAMI STRING IS TILTED. (A) ROTATED 4.4° COUNTERCLOCKWISE. (B) ROTATED 4.4° CLOCKWISE. $N = 10$.

transformation of a two-vertex origami string. We also successfully demonstrated that by changing dynamic input response, the origami string will enter different configurations, implying potential applications in controllable and rapid change of an overall envelop of origami devices.

Future designs could explore the effects of using stimuli responsive materials [35] that can change its elasticity. When using stimuli responsive materials to replace the springs, by changing temperature, for instance, we can change the stiffness of the elastic element on the cell so as to change the dynamic output of the stacked-Miura cell. In this way, we can provide more dynamic response to the origami string and achieve more transformations.

Even though we successfully demonstrated repeatable transformation of the origami string into different configurations via distinct inputs, we observed that the upper vertex of the origami string only resulted in a parallel configuration in both situations provided. To promote more complex behavior, we can change stiffness of the origami string (e.g. adding/subtracting barrel

hinges) or inertia of each plate (e.g. adding/subtracting weights).

As mentioned in the experimental section, the stacked-Miura cell is actuated by a tendon driven system powered by hand. A possible replacement could be a motor to pull the tendon but they are usually bulky. An alternative solution is to use a pouch motor [10, 23] that can be placed inside a stacked-Miura cell. As it inflates, it can cause the stacked-Miura cell to snap through. This method only requires a micro pneumatic pump to help the stacked-Miura cell reach the critical point, after which the latter can operate on its own. For reversibility, pneumatic artificial muscle (PAMs) [36] can be added. We expect that this approach could be applied in repeatedly and rapidly folding complex and large-scale origami devices, such as folding satellite panels [37], shape morphing aircraft wings [38,39], and origami-inspired antennas for wireless communication [40].

ACKNOWLEDGMENT

REFERENCES

[1] Hawkes, E., An, B., Benbernou, N. M., Tanaka, H., Kim, S., Demaine, E., Rus, D., and Wood, R. J., 2010. "Programmable matter by folding". *Proceedings of the National Academy of Sciences,* **107**(28), pp. 12441–12445.

[2] Kuribayashi, K., Tsuchiya, K., You, Z., Tomus, D., Umemoto, M., Ito, T., and Sasaki, M., 2006. "Self-deployable origami stent grafts as a biomedical application of ni-rich tini shape memory alloy foil". *Materials Science and Engineering: A,* **419**(1-2), pp. 131–137.

[3] Oliveira, M. B., Liu, C., Zhao, M., and Felton, S. M., 2018. "Design of a variable stiffness wrist brace with an origami structural element". In ASME 2018 Conference on Smart Materials, Adaptive Structures and Intelligent Systems, American Society of Mechanical Engineers, pp. V002T08A009–V002T08A009.

[4] Filipov, E. T., Tachi, T., and Paulino, G. H., 2015. "Origami tubes assembled into stiff, yet reconfigurable structures and metamaterials". *Proceedings of the National Academy of Sciences,* **112**(40), pp. 12321–12326.

[5] Dufour, L., Owen, K., Mintchev, S., and Floreano, D., 2016. "A drone with insect-inspired folding wings". In Intelligent Robots and Systems (IROS), 2016 IEEE/RSJ International Conference on, Ieee, pp. 1576–1581.

[6] Shigemune, H., Maeda, S., Hara, Y., Hosoya, N., and Hashimoto, S., 2016. "Origami robot: A self-folding paper robot with an electrothermal actuator created by printing". *IEEE/ASME Transactions on Mechatronics,* **21**(6), pp. 2746–2754.

[7] Shigemune, H., Maeda, S., Cacucciolo, V., Iwata, Y., Iwase, E., Hashimoto, S., and Sugano, S., 2017. "Printed

paper robot driven by electrostatic actuator". *IEEE Robotics and Automation Letters, 2*(2), pp. 1001–1007.

[8] Felton, S., Tolley, M., Demaine, E., Rus, D., and Wood, R., 2014. "A method for building self-folding machines". *Science, 345*(6197), pp. 644–646.

[9] Li, S., Vogt, D. M., Rus, D., and Wood, R. J., 2017. "Fluid-driven origami-inspired artificial muscles". *Proceedings of the National Academy of Sciences, 114*(50), pp. 13132–13137.

[10] Liu, C., Orlofsky, A., Kitcher, C., and Felton, S., 2019. "A self-folding pneumatic piston for mechanically robust origami robots". *IEEE Robotics and Automation Letters*.

[11] Miura, K., 1985. "Method of packaging and deployment of large membranes in space". *The institute of space and astronautical science report, 618*, pp. 1–9.

[12] Nishiyama, Y., 2012. "Miura folding: Applying origami to space exploration". *International Journal of Pure and Applied Mathematics, 79*(2), pp. 269–279.

[13] Molaei, A., Liu, C., Felton, S. M., and Martinez-Lorenzo, J., 2018. "Origami inspired reconfigurable antenna for wireless communication systems". *arXiv preprint arXiv:1805.10370.*

[14] Liu, X., Yao, S., Georgakopoulos, S. V., Cook, B. S., and Tentzeris, M. M., 2014. "Reconfigurable helical antenna based on an origami structure for wireless communication system". In 2014 IEEE MTT-S International Microwave Symposium (IMS2014), IEEE, pp. 1–4.

[15] Liu, Y., Boyles, J. K., Genzer, J., and Dickey, M. D., 2012. "Self-folding of polymer sheets using local light absorption". *Soft matter, 8*(6), pp. 1764–1769.

[16] Ionov, L., 2011. "Soft microorigami: self-folding polymer films". *Soft Matter, 7*(15), pp. 6786–6791.

[17] Paik, J. K., Hawkes, E., and Wood, R. J., 2010. "A novel low-profile shape memory alloy torsional actuator". *Smart Materials and Structures, 19*(12), p. 125014.

[18] Liu, C., Gomes, C. M., McDonald, K. J., Deravi, L. F., and Felton, S. M., 2018. "A chemo-mechatronic origami device for chemical sensing". In ASME 2018 Conference on Smart Materials, Adaptive Structures and Intelligent Systems, American Society of Mechanical Engineers, pp. V002T02A005–V002T02A005.

[19] Guo, W., Li, M., and Zhou, J., 2013. "Modeling programmable deformation of self-folding all-polymer structures with temperature-sensitive hydrogels". *Smart Materials and Structures, 22*(11), p. 115028.

[20] Gomes, C. M., Liu, C., Paten, J. A., Felton, S. M., and Deravi, L. F., 2019. "Protein-based hydrogels that actuate self-folding systems". *Advanced Functional Materials*, p. 1805777.

[21] Bassik, N., Abebe, B. T., Laflin, K. E., and Gracias, D. H., 2010. "Photolithographically patterned smart hydrogel based bilayer actuators". *Polymer, 51*(26), pp. 6093–6098.

[22] Liu, C., and Felton, S. M., 2017. "A self-folding robot arm for load-bearing operations". In Intelligent Robots and Systems (IROS), 2017 IEEE/RSJ International Conference on, IEEE, pp. 1979–1986.

[23] Niiyama, R., Rus, D., and Kim, S., 2014. "Pouch motors: Printable/inflatable soft actuators for robotics". In Robotics and Automation (ICRA), 2014 IEEE International Conference on, IEEE, pp. 6332–6337.

[24] Zuliani, F., Liu, C., Paik, J., and Felton, S. M., 2018. "Minimally actuated transformation of origami machines". *IEEE Robotics and Automation Letters, 3*(3), pp. 1426–1433.

[25] Liu, C., and Felton, S. M., 2018. "Transformation dynamics in origami". *Physical review letters, 121*(25), p. 254101.

[26] Waitukaitis, S., Menaut, R., Chen, B. G.-g., and van Hecke, M., 2015. "Origami multistability: From single vertices to metasheets". *Physical review letters, 114*(5), p. 055503.

[27] Chen, B. G.-g., and Santangelo, C. D., 2018. "Branches of triangulated origami near the unfolded state". *Physical Review X, 8*(1), p. 011034.

[28] Stern, M., Pinson, M. B., and Murugan, A., 2017. "The complexity of folding self-folding origami". *Physical Review X, 7*(4), p. 041070.

[29] Li, S., and Wang, K., 2015. "Fluidic origami with embedded pressure dependent multi-stability: a plant inspired innovation". *Journal of The Royal Society Interface, 12*(111), p. 20150639.

[30] Burgert, I., and Fratzl, P., 2009. "Actuation systems in plants as prototypes for bioinspired devices". *Philosophical Transactions of the Royal Society A: Mathematical, Physical and Engineering Sciences, 367*(1893), pp. 1541–1557.

[31] Li, S., and Wang, K., 2016. "Plant-inspired adaptive structures and materials for morphing and actuation: a review". *Bioinspiration & biomimetics, 12*(1), p. 011001.

[32] Fang, H., Li, S., Ji, H., and Wang, K., 2017. "Dynamics of a bistable miura-origami structure". *Physical Review E, 95*(5), p. 052211.

[33] Cazottes, P., Fernandes, A., Pouget, J., and Hafez, M., 2009. "Bistable buckled beam: modeling of actuating force and experimental validations". *Journal of Mechanical Design, 131*(10), p. 101001.

[34] Kamrava, S., Mousanezhad, D., Felton, S. M., and Vaziri, A., 2018. "Programmable origami strings". *Advanced Materials Technologies, 3*(3), p. 1700276.

[35] Shan, W., Lu, T., and Majidi, C., 2013. "Soft-matter composites with electrically tunable elastic rigidity". *Smart Materials and Structures, 22*(8), p. 085005.

[36] Tondu, B., and Lopez, P., 1997. "The mckibben muscle and its use in actuating robot-arms showing similarities with human arm behaviour". *Industrial Robot: An International Journal, 24*(6), pp. 432–439.

[37] Zirbel, S. A., Lang, R. J., Thomson, M. W., Sigel, D. A., Walkemeyer, P. E., Trease, B. P., Magleby, S. P., and How-

ell, L. L., 2013. "Accommodating thickness in origami-based deployable arrays". *Journal of Mechanical Design, 135*(11), p. 111005.

[38] Vos, R., and Barrett, R., 2011. "Mechanics of pressure-adaptive honeycomb and its application to wing morphing". *Smart Materials and Structures, 20*(9), p. 094010.

[39] Baek, S.-M., Lee, D.-Y., and Cho, K.-J., 2016. "Curved compliant facet origami-based self-deployable gliding wing module for jump-gliding". In ASME 2016 International Design Engineering Technical Conferences and Computers and Information in Engineering Conference, American Society of Mechanical Engineers, p. V05BT07A028.

[40] Fuchi, K., Buskohl, P. R., Joo, J. J., and Reich, G. W., 2016. "Control of rf transmission characteristics through origami design". In ASME 2016 International Design Engineering Technical Conferences and Computers and Information in Engineering Conference, American Society of Mechanical Engineers, pp. V05BT07A018–V05BT07A018.